Electronic Supplementary Material (ESI) for Nanoscale.

Supporting Information

Topological Transformation of LDH Nanosheets to Highly Dispersed PtNiFe Nanoalloys that Enhances CO Oxidation Performance

Junfang Ding†, Liping Li†, Ye Wang†, Huixia Li†, Min Yang†, Guangshe Li†*

†State Key Laboratory of Inorganic Synthesis and Preparative Chemistry, College of Chemistry, Jilin University, Changchun 130012, P.R. China

*E-mail: guangshe@jlu.edu.cn.

Table of Contents

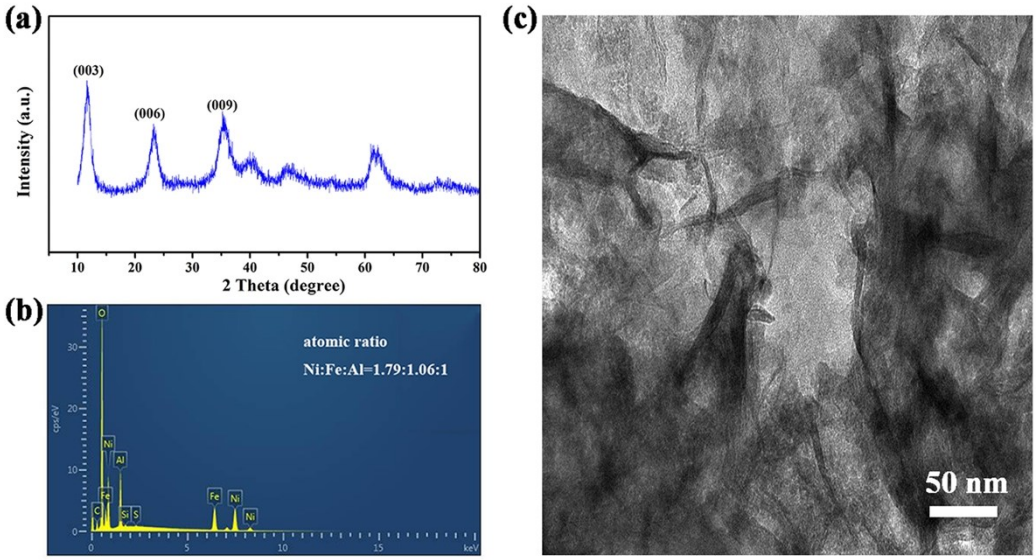

Figure S1 (a) XRD pattern, (b) EDX spectrum, and (c) TEM image of the as-synthesized NiFeAl-LDH precursor.

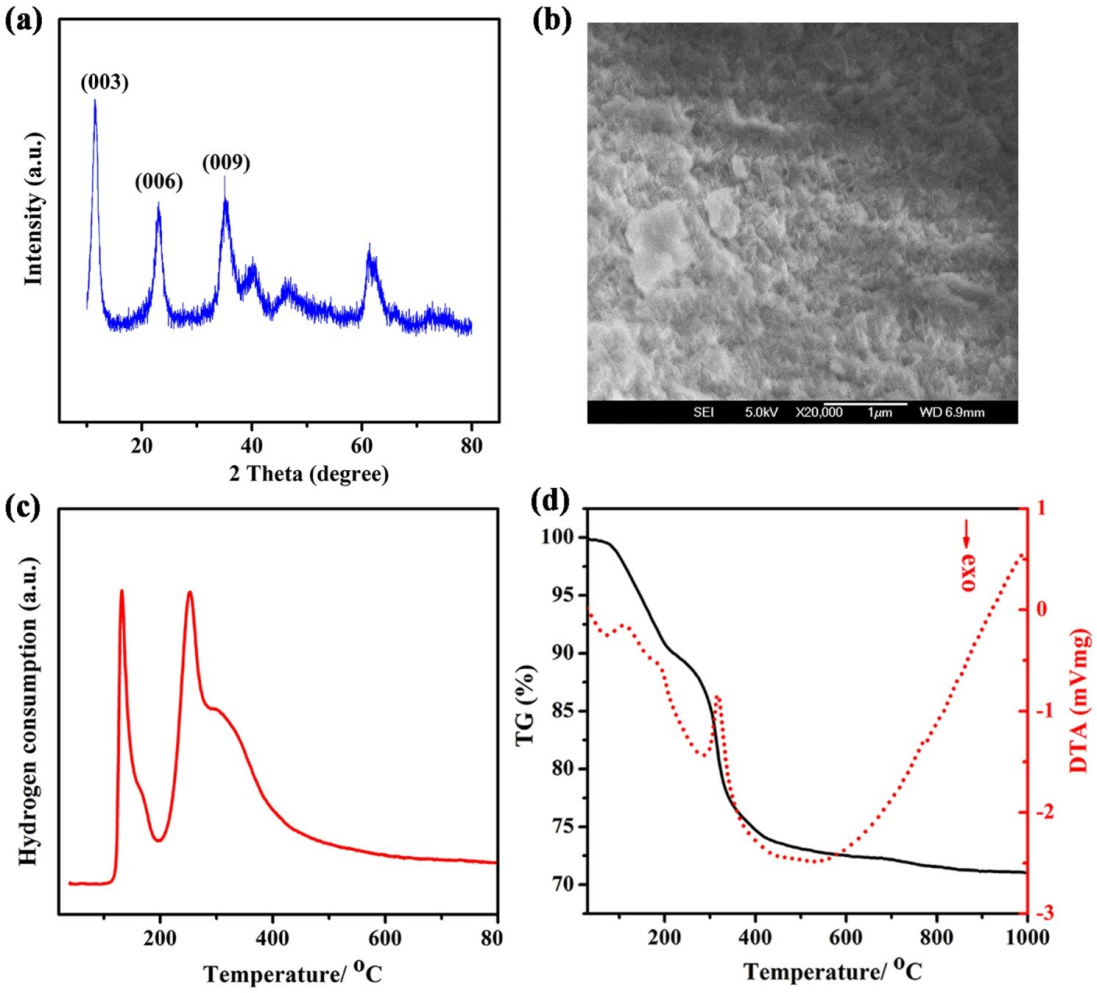

Figure S2 (a) XRD patterns; (b) SEM image; (c) H_2-TPR profiles; and (d) TGA-DSC curves of Pt/NiFeAl-LDH precursor.

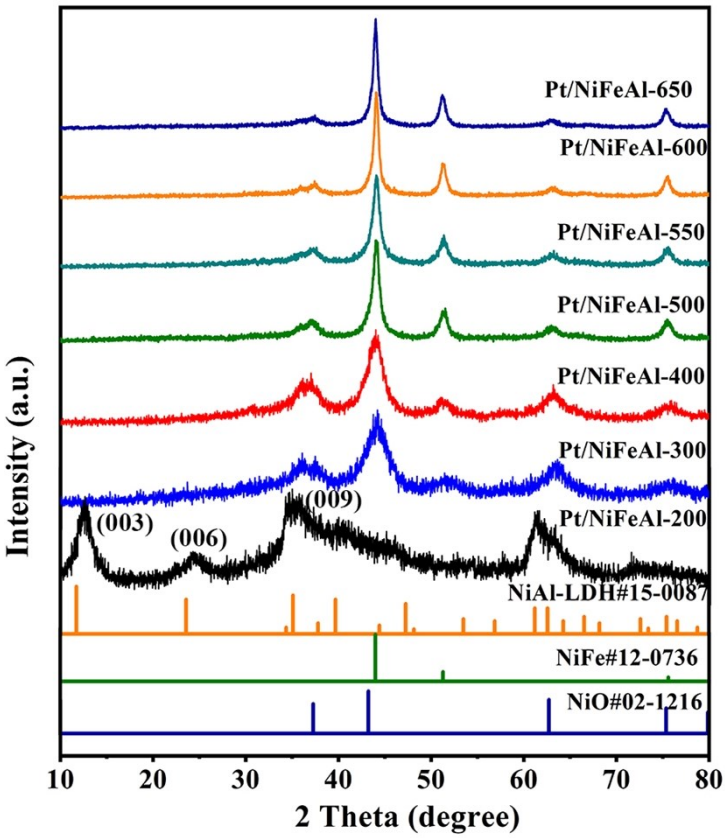

Figure S3 XRD patterns of the samples Pt/NiFeAl-x (x represents reduction temperature).

The XRD peaks of NiFeAl-LDH nanosheets can be accordingly ascribed to the NiAl-LDH phase (JCPDS card No. 15-0087, *R-3m(116): a=b=3.025, c=22.595*). Owing to the introduction of Fe species, resulting in lattice distortion, the positions of (003), (006) and (009) peaks slightly shifted.

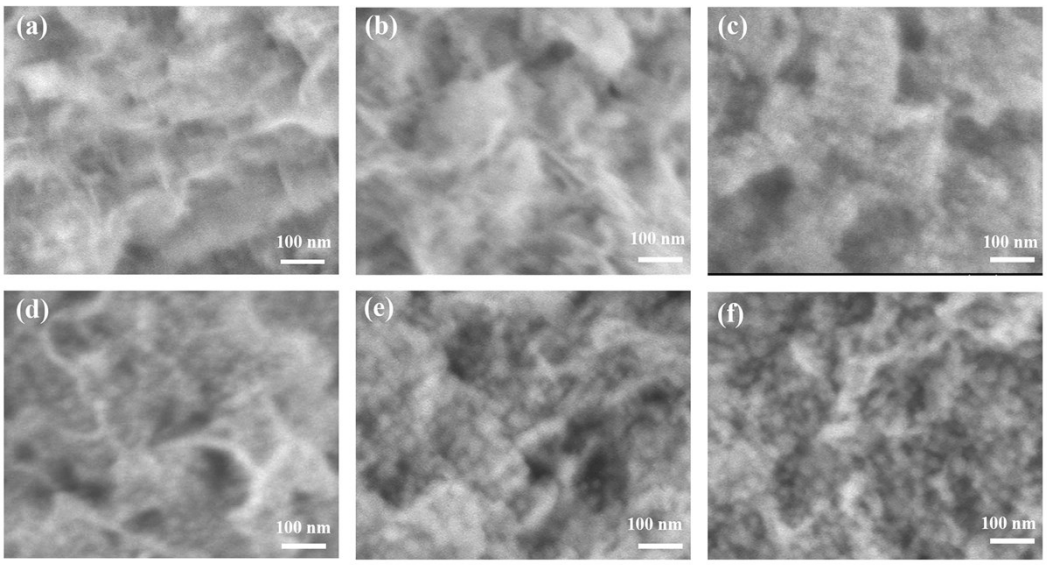

Figure S4 Enlarged SEM images of the samples Pt/NiFeAl-x: (a) x=300; (b) x=400; (c) x=500; (d) x=550; (e) x=600; and (f) x=650.

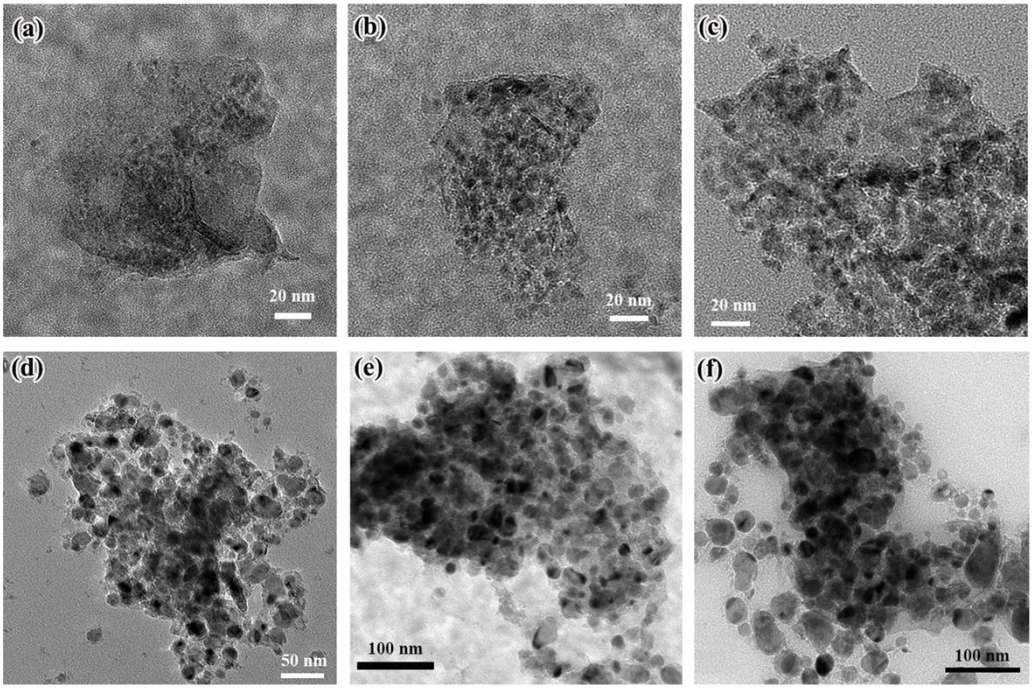

Figure S5 TEM image of the samples Pt/NiFeAl-x: (a) x=200; (b) x=300; (c) x=400; (d) x=500; (e) x=550; and (f) x=650.

As seen in Figure S5a, sample Pt/NiFeAl-200 exhibits a uniform, silk-like, 2D nanosheet structure with a large lateral size of about several micrometers. Pt particles are uniformly dispersed on NiFeAl LDH support, showing an average size around 3 nm. When the reduction temperature increased to 300 ^{o}C, NiFe alloy nanoparticles appeared, evenly distributed on nanosheet support. As expected, NiFe alloy nanoparticles gradually became larger as reduction temperature increases.

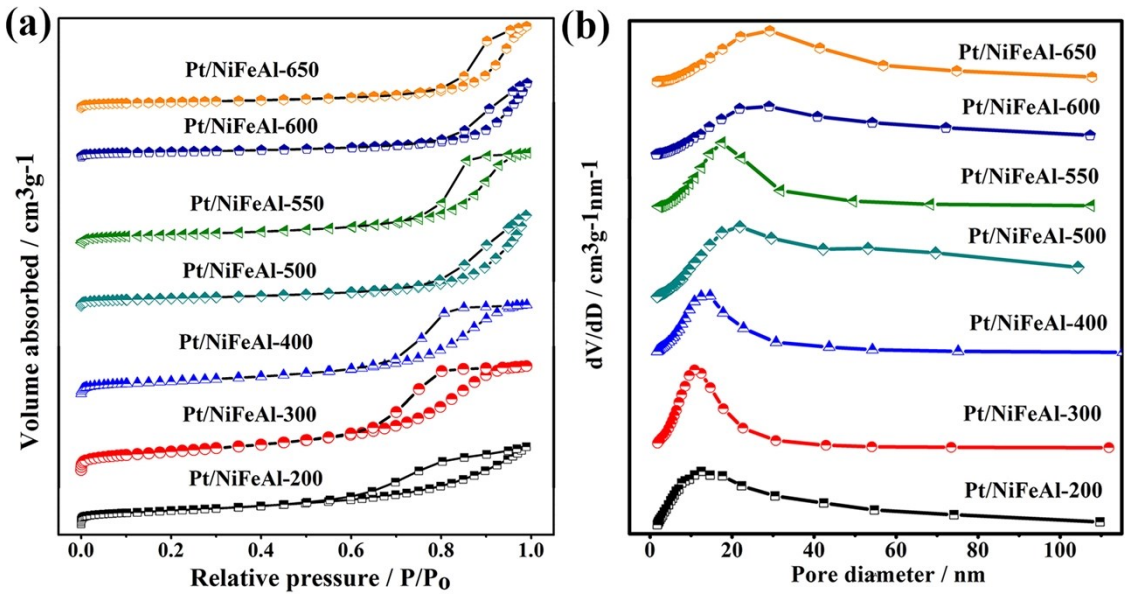

Figure S6 N_2 adsorption-desorption isotherms and pore size distributions calculated from the desorption branch of the samples Pt/NiFeAl-x.

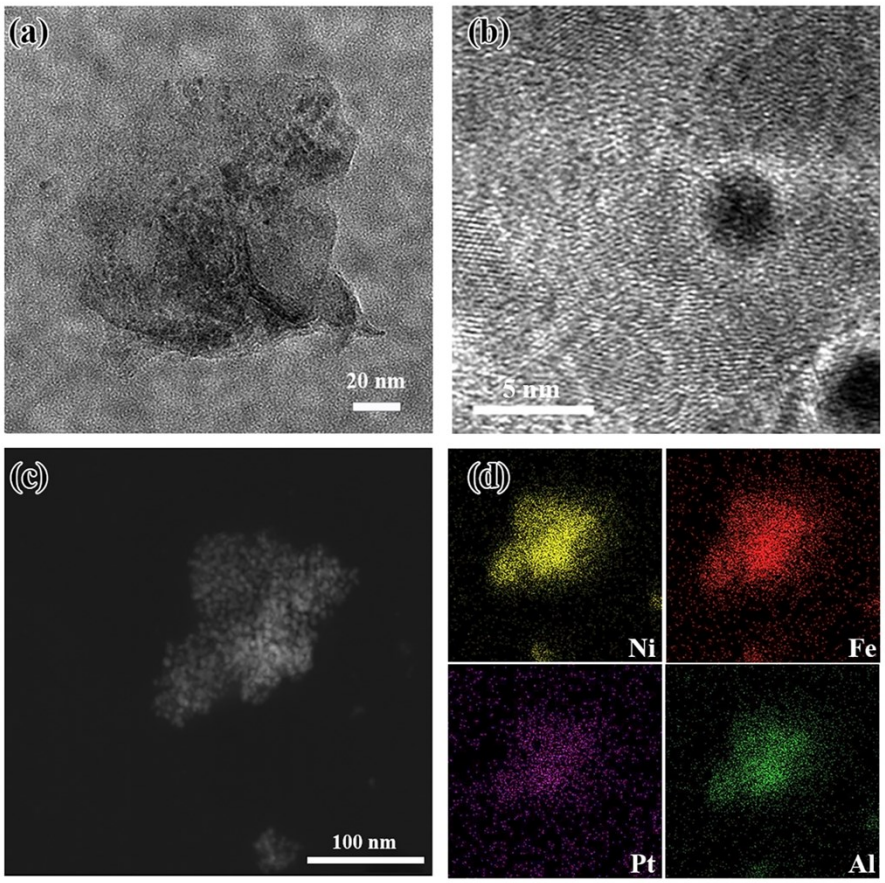

Figure S7 (a) TEM image; (b) HRTEM image; (c) High-angle annular dark-field scanning TEM image; and (d) EDS mapping for Ni, Fe, Pt, Al of the sample Pt/NiFeAl-x at x=200.

For x=200, a silk-like 2D nanosheet structure and Pt particles were indicated uniformly dispersed on NiFeAl LDH support (Figure S7). Since there is no NiFe alloy for x=200, those nanoparticles seen in HRTEM image could be identified as Pt nanoparticles. Form STEM-EDS mapping in Figures S7c and 7d, Ni, Fe and Al elements are homogeneously distributed across the whole nanosheet, and no distinct aggregation signals of Pt species were detected in the image.

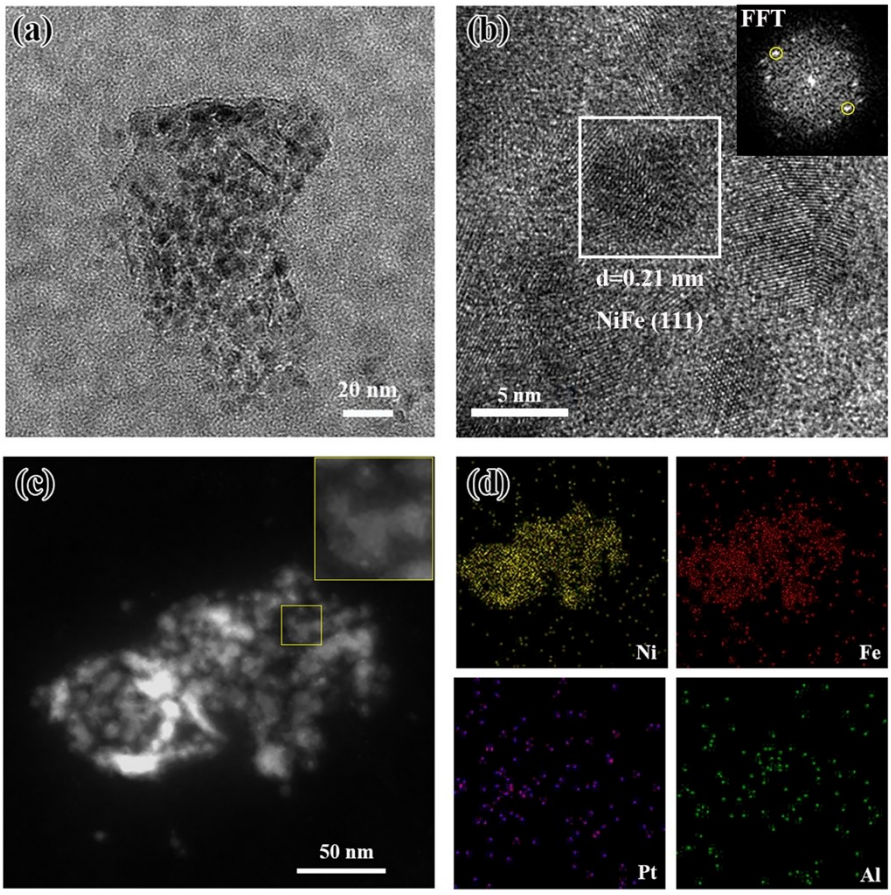

Figure S8 (a) TEM image; (b) HRTEM image, inset shows the FFT pattern of rectangle region; (c) High-angle annular dark-field scanning TEM image, Inset shows the enlarged image of rectangle region; and (d) EDS mapping for Ni, Fe, Pt, Al of the sample Pt/NiFeAl-x at x=300.

For x=300, the original nanosheet morphology of the precursor (NiFeAl-LDH) was maintained, and NiFe alloy appeared and was evenly distributed on nanosheet support (Figure S8a). Those nanoparticles seen in HRTEM diagram cannot be distinguished to be Pt or NiFe alloy. A HRTEM image of the rectangle region in Figure S8b indicates a set of clear crystalline lattice of 2.1 Å, which could be assigned to the crystal planes (111) of NiFe alloy. Pt clusters of higher contrast can be clearly seen in the enlarged HAADF-STEM image. No distinct aggregation signals of Pt species were detected in the STEM-EDS mapping.

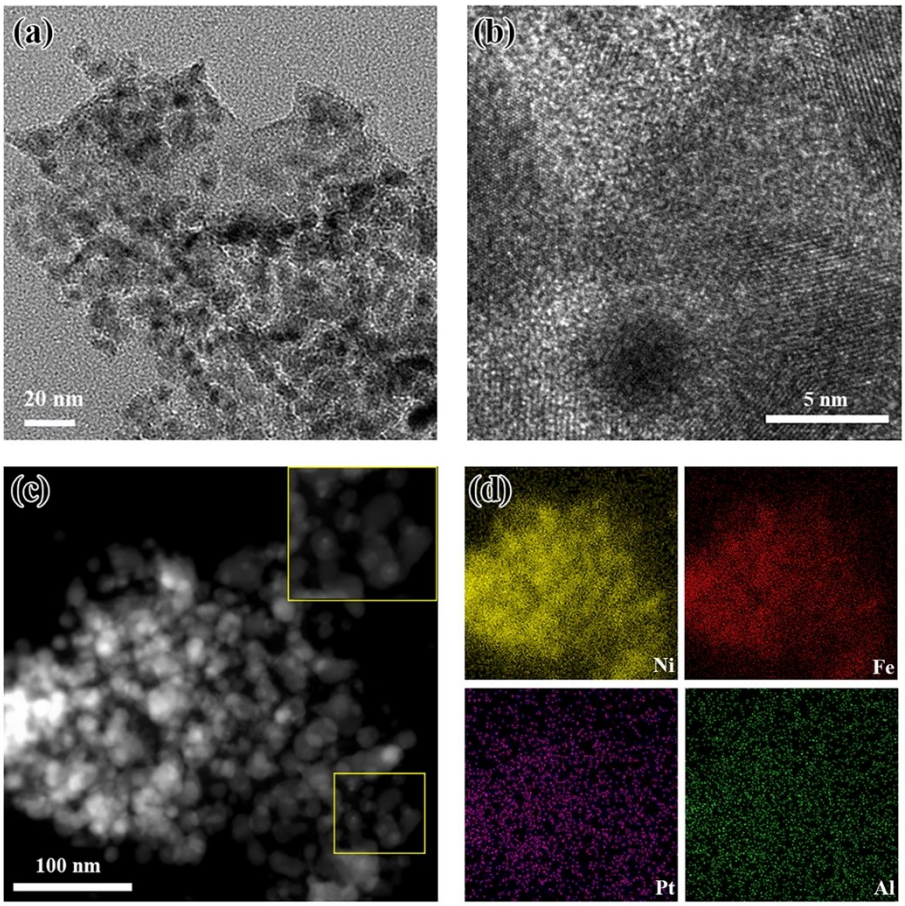

Figure S9 (a) TEM image; (b) HRTEM image; (c) High-angle annular dark-field scanning TEM image, Inset shows the enlarged image of rectangle region; and (d) EDS mapping for Ni, Fe, Pt, Al of the sample Pt/NiFeAl-x at x=400.

For x=400, the nanosheet morphology of the precursor (NiFeAl-LDH) was maintained with the appearance of NiFe alloys (Figure S9a). Pt clusters of higher contrast were clearly seen in the enlarged HAADF-STEM image. No distinct aggregation signals of Pt species were detected in the STEM-EDS mapping.

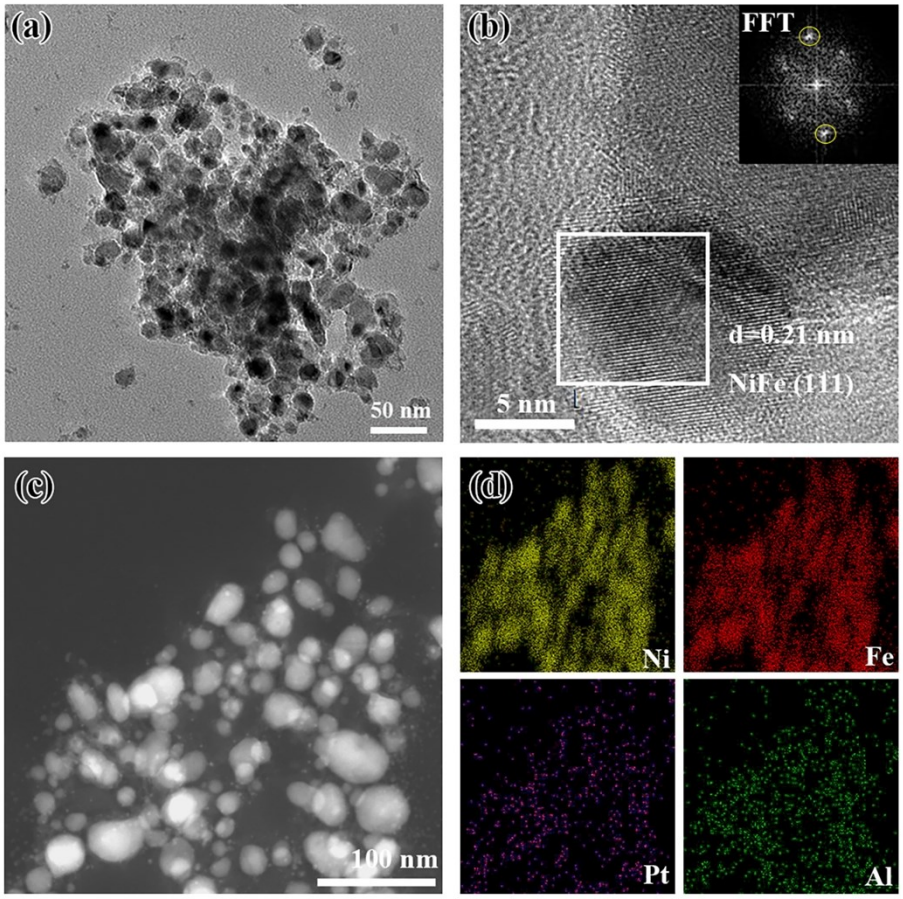

Figure S10 (a) TEM image; (b) HRTEM image, inset shows the FFT pattern of rectangle region; (c) High-angle annular dark-field scanning TEM image, Inset shows the enlarged image of rectangle region; and (d) EDS mapping for Ni, Fe, Pt, Al of the sample Pt/NiFeAl at x=500.

For x=500, the original nanosheet morphology of the precursor (NiFeAl-LDH) could be maintained to a certain extent with the appearance of NiFe alloys (Figure S10a). NiFe alloy particles for x=500 grew larger compared with those for x=200-400. Pt clusters of higher contrast were clearly seen in the enlarged HAADF-STEM image. No distinct aggregation signals of Pt species were detected in the STEM-EDS mapping.

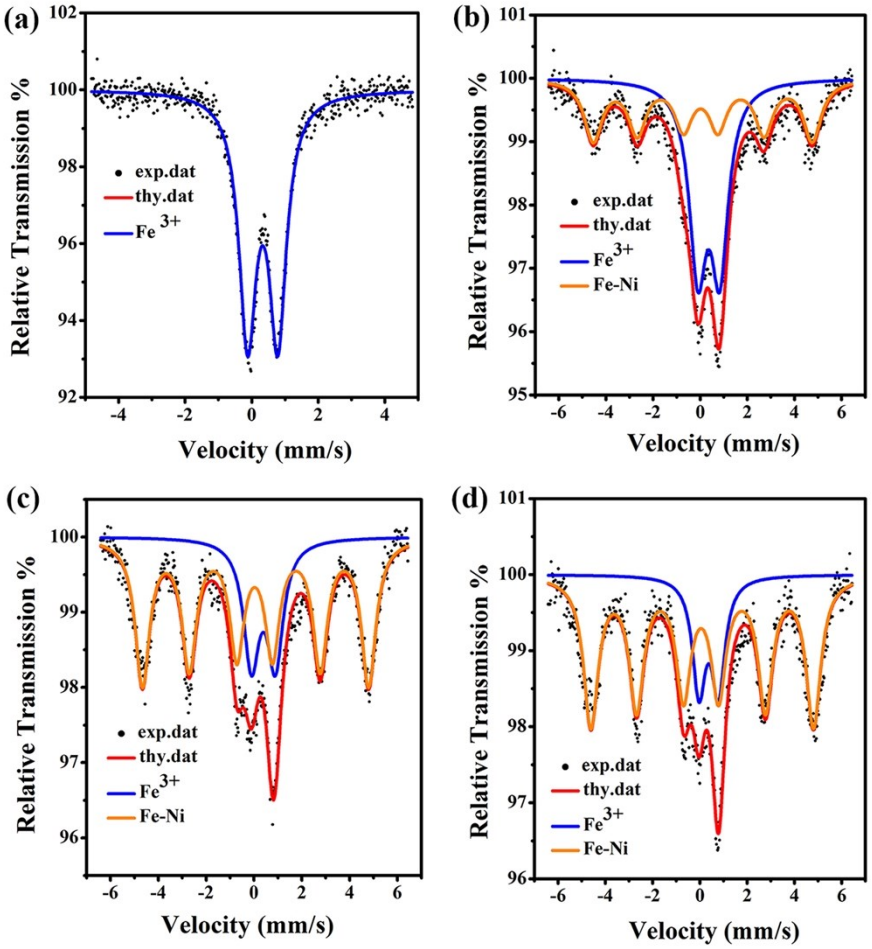

Figure S11 Mössbauer spectra for the samples Pt/NiFeAl-x at (a) x=300; (b) x=500; (c) x=550; and (d) x=650.

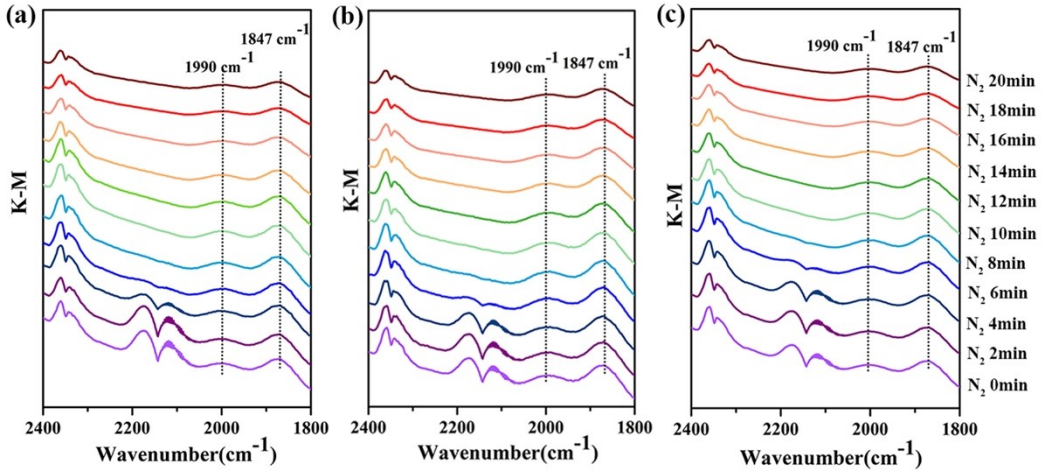

Figure S12 Temporal evolutions of the DRIFTS spectra after saturation adsorption of CO on the samples Pt/NiFeAl-x: (a) x=500, (b) x=550 and (c) x=650 during a continuous N_2 flushing.

Table S1 Comparisons of CO oxidation activities of the sample Pt/NiFeAl-x at x=600 with those of catalysts reported in literatures.

Sample	Amount of catalyst (mg)	Space Velocity (h^{-1})	Feed gas	T_{100}	Reference
Pt/NiFeAl-600	50	60 000	1% CO, 20% O_2, He balance	100 °C	This work
AuCu/Al_2O_3	Undefined	3 000 000	1% CO, 6% O_2, He balance	200 °C	1
PdNi@HNTs	50	72 000	3.5% CO, 20% O_2, Ar balance	122 °C	2
Cu-Rh_{1-3}NSUrs	100	Undefined	2% CO, 2 % O_2, N_2 balance	140 °C	3
Pd-4.6/Co_3O_4	50	Undefined	1% CO, 1% O_2, Ar balance	160 °C	4
Pt/Fe_3O_4	50	240 000	1500 ppm CO, 10% O_2, N_2 balance	150 °C	5
Pt-$Ni_{0.3}Co_{2.7}O_4$	55	15 000	1% CO, 20% O_2, N_2 balance	120 °C	6
Pt-Co_3O_4	55	15 000	1% CO, 20% O_2, N_2 balance	260 °C	6
Pt-NiO	55	15 000	1% CO, 20% O_2, N_2 balance	270 °C	6
0.2Pt/m-Al_2O_3-H_2	100	24 000 000	2.5% CO, 2.5% O_2, Ar balance	280 °C	7
Pt/CeO_2-S	30	200 000	0.4 % CO, 10 % O_2, Ar balance	148 °C	8
Leached PtNi/CB	Undefined	30 000	1% CO, 20% O_2, He balance	140 °C	9
Pt/C70G30	200	16 000	0.2% CO, 0.9% O_2, He balance	250 °C	10
Pt/DBD-WO_3	Undefined	Undefined	1% CO, 20% O_2, N_2 balance	140 °C	11

References:

(1) S. Najafishirtari, R. Brescia, P. Guardia, S. Marras, L. Manna, M. Colombo, *ACS Catal,* **2015**, 5, 2154-2163.

(2) Y. H. Ahmad, A. T. Mohamed, W. M. I. Hassan, A. Soliman, K. A. Mahmoud, A. S. Aljaber, S. Y. Al-Qaradawi, *Appl. Surf. Sci.,* **2019**, 493, 70-80.

(3) W. Wang, Z. Cao, K. Liu, J. Chen, Y. Wang, S. Xie, *Nano Lett,* **2017**, 17, 7613-7619.

(4) R. Huang, K. Kim, H. J. Kim, M. G. Jang, J. W. Han, *ACS Appl.Nano. Materials,* **2020,** 3, 486-495.

(5) L. Ma, X. Chen, J. Li, H. Chang, J. W. Schwank, *Catal. Today,* https://doi.org/10.1016/j.cattod.2019.06.055

(6) X. Wang, D. Liu, F. Wang, J. Li, J. Zhen, H. Zhang, *ChemPlusChem,* **2015**, *80*, 1241-1244.

(7) Z. Zhang, Y. Zhu, H. Asakura, B. Zhang, J. Zhang, M. Zhou, Y. Han, T. Tanaka, A. Wang, T. Zhang, N. Yan, *Nat Commun,* **2017**, *8*, 16100.

(8) L. Nie, D. Mei, H. Xiong, B. Peng, Z. Ren, X. I. P. Hernandez, A. DeLaRiva, M. Wang, M. H. Engelhard, L. Kovarik, A. K. Datye, Y. Wang, *Science,* **2017**, *358*, 1419-1423.

(9) R. Mu, Q. Fu, H. Xu, H. Zhang, Y. Huang, Z. Jiang, S. Zhang, D. Tan, X. Bao, *J. Am. Chem. Soc.,* **2011**, *133*, 1978-1986.

(10) C. Meephoka, C. Chaisuk, P. Samparnpiboon, P. Praserthdam, *Catal. Commun,* **2008**, *9*, 546-550.

(11) J. Wang, Z. Wang, C. J. Liu, *ACS Appl. Mater. Interfaces,* **2014**, *6*, 12860-12867.